Atmos. Chem. Phys. Discuss., 3, 1183–1212, 2003
www.atmos-chem-phys.org/acpd/3/1183/

Atmospheric Chemistry and Physics Discussions

OH in the coastal boundary layer of Crete during MINOS: Measurements and relationship with ozone photolysis

H. Berresheim[1], C. Plass-Dülmer[1], T. Elste[1], N. Mihalopoulos[2], and F. Rohrer[3]

[1]German Weather Service, Meteorological Observatory Hohenpeissenberg, Germany
[2]University of Crete, Environmental Chemical Processes Laboratory, Heraklion, Greece
[3]Research Center Jülich, Institute for Chemistry and Dynamics of the Geosphere II, Jülich, Germany

Received: 4 February 2003 – Accepted: 20 February 2003 – Published: 27 February 2003

Correspondence to: H. Berresheim (harald.berresheim@dwd.de)

Abstract

Hydroxyl radical (OH) concentrations were measured in August 2001 at Finokalia Station on the northeastern coast of Crete during the Mediterranean Intensive Oxidant Study (MINOS). OH was measured based on selected ion chemical ionization mass spectrometry (SI/CIMS) with a time resolution of 30 s and signal integration of 5 min. The corresponding accuracy, precision, and detection limit were 20% (1σ), 11% (1σ), and 2.4×10^5 molecules cm^{-3} (2σ), respectively. OH levels showed a strong diurnal variability with high maxima (approximately 2×10^7 molecules cm^{-3}) occurring around 13:30 LT (10:30 UTC) and nighttime values below the detection limit. Daily 24-hour average concentrations varied between $3.6 - 6.7 \times 10^6$ cm^{-3}. For the total measurement period (6-21 August) the mean and standard deviation were $4.5 \pm 1.1 \times 10^6$ cm^{-3}. The OH data set is analyzed based on a classification into three periods: I: 6–8 August, II: 9–11 August, III: 13–18 August. For each of the three periods the measured OH concentrations are described by the empirical function $[OH] = a\ J(O^1D)^{0.68}$, with $J(O^1D)$ being the ozone photolysis frequency and $a = 1.4 \times 10^{10}$ s cm^{-3}, 1.7×10^{10} s cm^{-3}, and 2.2×10^{10} s cm^{-3}, respectively. It is shown that this relationship is consistent with a CH_4-CO box model yielding a corresponding exponent of 0.70. Taking into account the estimated precision of the OH measurements this empirical function explains 99% of the observed variance of OH.

1. Introduction

One of the major goals of the Mediterranean Intensive Oxidant Study (MINOS) was to investigate the effect of anthropogenic air pollution on the budgets of atmospheric oxidants (e.g. ozone) over the Mediterranean region (Lelieveld et al., 2002a). The concentration of the most reactive oxidant species in the troposphere, the hydroxyl radical (OH), depends strongly on the ambient levels of ozone and water vapour and on solar irradiance. In the remote atmosphere OH is primarily produced via ozone

ACPD
3, 1183–1212, 2003

photolysis at wavelengths less than about 330 nm (Matsumi et al., 2002) followed by reaction of the electronically excited $O(^1D)$ atom with water vapour:

$$O_3 + h\nu \longrightarrow O(^1D) + O_2 \quad \text{(R1)}$$

$$O(^1D) + M \longrightarrow O(^3P) + M\,(M = N_2,\ O_2) \quad \text{(R2)}$$

$$O(^1D) + H_2O \longrightarrow 2\,OH. \quad \text{(R3)}$$

From the above reaction scheme a primary OH production rate, P(OH), can be derived:

$$P(OH) = \frac{2J(O^1D)[O_3]k_{H_2O}[H_2O]}{k_{O_2}[O_2] + k_{N_2}[N_2] + k_{H_2O}[H_2O]}, \quad (1)$$

where $J(O^1D)$ is the ozone photolysis frequency, and k_{O_2}, k_{N_2}, and k_{H_2O} are the rate coefficients for reactions (R2) and (R3), respectively. The average tropospheric lifetime of OH is less than 1 s due to its relatively fast reactions with a large number of both anthropogenic and natural compounds. Major sinks for OH are the reactions with CO, CH_4, and non-methane hydrocarbons (NMHCs) in which peroxy radicals (HO_2, RO_2; R = organic rest) are produced as intermediate products. In addition, HO_2 is also produced from the photolysis of formaldehyde, HCHO. In turn, these peroxy radicals can be involved in further reactions leading back to OH (secondary OH source), i.e. OH can be recycled via HO_2 by reaction with NO or O_3:

$$NO + HO_2 \longrightarrow NO_2 + OH \quad \text{(R4)}$$

$$O_3 + HO_2 \longrightarrow 2\,O_2 + OH. \quad \text{(R5)}$$

Important loss processes for the sum of OH and HO_2 radicals (denoted here as HO_x) are:

$$NO_2 + OH + M \longrightarrow HNO_3 + M \quad (M = N_2,\ O_2) \quad \text{(R6)}$$

ACPD
3, 1183–1212, 2003

and radical self-reactions

$$OH + HO_2 \longrightarrow H_2O + O_2 \quad \text{(R7)}$$

$$HO_2 + HO_2 \longrightarrow H_2O_2 + O_2 \quad \text{(R8)}$$

$$HO_2 + RO_2 \longrightarrow ROOH + O_2 \quad \text{(R9)}$$

The latter dominate in relatively clean NO_x-depleted environments such as the remote marine atmosphere (NO_x = NO + NO_2), the former in relatively polluted air (e.g. Platt et al., 2002; Lelieveld et al., 2002b).

As part of the MINOS experiment daily measurements of ambient OH concentrations were conducted during 6–22 August 2001, at the ground level station Finokalia on the northeastern coast of Crete. Specific objectives of these measurements were: (1) to study the atmospheric oxidation capacity and production of OH in the Mediterranean boundary layer, and (2) to provide a data base of diurnally measured OH profiles for detailed modelling of the local and regional photochemistry. In the present work, we first discuss experimental details, and the results and uncertainties of the OH measurements. Next, the corresponding O_3, CO, meteorological and photolysis frequency data are used to distinguish three periods within the OH data set. In the final part, the variance in the OH data is analyzed for each of these periods by both an empirical functional and a box model approach. The paper concludes with a quantitative assessment of individual contributions to the observed OH variance and their relationship with ozone photolysis. For a comprehensive and detailed photochemical model analysis of the OH data the reader is referred to the companion paper by Baboukas et al. (2003).

2. Experimental

2.1. OH measurements

Atmospheric OH concentrations were measured by selected ion / chemical ionization mass spectrometry (SI/CIMS) previously developed by Eisele and coworkers (Tanner

ACPD
3, 1183–1212, 2003

et al., 1997; Eisele and Tanner, 1991). During the MINOS campaign the system was installed in a mobile field laboratory (container) at Finokalia station (35°19′ N, 25°40′ E) on the northeastern coast of Crete. The container was deployed on a plateau near the edge of a cliff approximately 100 m above the coastline and some 20 m vertical distance below the summit laboratory operated by the University of Crete (ECPL). The Finokalia site is located about 80 km east of Heraklion and at least 20 km away from major road traffic and small cities further south. The surrounding vegetation is sparse and consists mainly of some herbs and low bushes. OH was measured continuously between 6–22 August 2001. In addition, ambient concentrations of H_2SO_4 and gaseous methane sulfonic acid, MSA, were measured. For the results and interpretation of the sulfur measurements see Bardouki et al. (2003) and Kanakidou et al. (2003). Short interruptions of the measurements occurred due to maintenance or power outage problems. The SI/CIMS system of Deutscher Wetterdienst (DWD; German Weather Service) has been described in detail by Berresheim et al. (2000). A brief outline of the measurement technique and of the system's performance during MINOS is given here.

Ambient air is sampled at approximately 10 l min^{-1} into the ion reaction region of the system where neutral sample molecules such as H_2SO_4 are ionized at atmospheric pressure by charge transfer reactions with NO_3^- core ions. The NO_3^- ions are produced in a separate sheath gas by a radioactive ^{241}Am source and are subsequently focussed by electrical fields to the sample flow axis. H_2SO_4 and MSA molecules directly react with NO_3^- yielding the corresponding HSO_4^- and MSA^- product ions. To measure OH, excess $^{34}SO_2$ is added to the sample flow before the ionization region. The SO_2 completely titrates the sampled OH within approximately 20 ms producing heavy isotope $H_2^{34}SO_4$ molecules which in turn react with NO_3^- to produce $H^{34}SO_4^-$ product ions. These differ from the $H^{32}SO_4^-$ ions derived from ambient H_2SO_4 by two mass units. The OH background signal is produced by adding high purity propane to the sample air/SO_2 mixture such that all OH is now scavenged by reaction with propane instead of SO_2. A fraction of the remaining NO_3^- ions and the newly formed product ions are forced by electrical fields through a 200 μm diameter aperture into a differen-

ACPD
3, 1183–1212, 2003

tially pumped vacuum region where they are first stripped of neutral ligand molecules, then mass-filtered by a quadrupole (at approximately 2×10^{-5} hPa pressure), and finally detected by an electron multiplier. The OH concentration is determined from the corresponding $H^{34}SO_4^-$ to NO_3^- signal ratio and a calibration factor F according to:

$$[OH] = F(H^{34}SO_4^-/NO_3^-). \quad (2)$$

During the MINOS campaign calibration measurements were made regularly every hour using a calibration unit which emits filtered UV light at $\lambda = 184.9$ nm into the air flow in front of the sample tube. The UV light photolyzes the water vapor molecules in the sampled air yielding OH concentrations in the range $0.3 - 1 \times 10^8$ cm^{-3}. The generated OH concentrations are determined based on the known H_2O absorption cross section (Cantrell et al., 1997) and concurrent measurements of $[H_2O]$ and the UV photon flux (for details, see Berresheim et al., 2000). OH was measured at 30 s time resolution and the corresponding signals were averaged over 5 min intervals. The measurements were corrected by a factor of 0.82 to account for errors resulting from chemically induced changes in the CIMS sample inlet and titration zones. This correction was based on an iterative approach previously described by Berresheim et al. (2000) and Tanner et al. (1997) using average mixing ratios of NO_x (400 pptv; 1 pptv = 10^{-12}), O_3 (65 ppbv; 1 ppbv = 10^{-9}) and CO (160 ppbv) measured at Finokalia during MINOS (see also Table 1; Lange et al., 2003; Salisbury et al., 2003). In addition, ambient air mixing ratios of CH_4, H_2, and HCHO were assumed to be 1900 ppbv, 550 ppbv, and 1 ppbv, respectively. The latter assumption is supported by airborne HCHO measurements in the lower marine boundary layer during MINOS (Kormann et al., 2003; Lelieveld et al., 2002a) and measurements performed at Finokalia during summer time in 2000 (Economou and Mihalopoulos, unpublished data). The sensitivity of the CIMS instrument showed no significant trend during the campaign. Therefore, all OH measurements during the MINOS campaign were evaluated by applying a median calibration factor F of 3.12×10^9 cm^{-3}. This value already includes the correction by a factor of 0.82 described above.

ACPD
3, 1183–1212, 2003

The precision of the ambient air OH measurements is essentially determined by the signal count statistics of the CIMS instrument, wind turbulence, and chemically induced variability. For the MINOS campaign the precision was estimated by first determining the reproducibility of the OH calibration. A standard deviation for F of 14% (1σ) was obtained. Next, contributions from calibration-specific variabilities (UV photon flux and H_2O measurements) were determined and subtracted yielding an estimated precision of 11% (1σ) for the ambient OH measurements. The detection limit for OH was calculated to be $2.4 \times 10^5\,cm^{-3}$ (2σ) based on signal count statistics as described by Berresheim et al. (2000).

Measurement accuracy accounts for both precision and systematic uncertainties. The latter were determined to amount to a total of 15% (1σ) based on contributions from the calibration of the cathodes (8%, 1σ), the corresponding UV photon flux measurements (8%, 1σ), the flow velocity in the illuminated zone (8%, 1σ), and minor contributions (6%, 1σ) from uncertainties in the [H_2O] measurements, the H_2O absorption cross section, and the median value of F. As a final result, the total accuracy for individual 5 min integrated OH measurements during the MINOS campaign is estimated to be 20% (1σ).

2.2. Photolysis frequencies and ancillary measurements

Photolysis frequencies $J(O^1D)$ and $J(NO_2)$ were measured continuously by filter radiometers (Meteorologie Consult, Germany). The accuracy of the $J(NO_2)$ filter radiometer was determined to be 15%, precision better than 3%. For the $J(O^1D)$ measurements one sensor pointing upward was used (upper 2π sr). Occasional tests reversing the direction of the sensor showed that the irradiance reflected from the ground (lower 2π sr) contributed about 10% of the $J(O^1D)$ value measured in upward direction. Therefore, total $J(O^1D)$ values were obtained by augmenting the upwardly measured values by 10%. The $J(O^1D)$ sensor was calibrated against a spectral radiometer in November 2001 (Bohn, Research Center Jülich, personal communication, 2002). The accuracy of the instrument after calibration was estimated to be 15%, precision is better

ACPD
3, 1183–1212, 2003

than 3%.

NO_2 was measured by differential optical long-path absorption (DOAS) as described in detail by Lange et al. (2003). O_3 was measured using a Thermo Analyser Model 49C and CO was monitored every 15 min by gas chromatography equipped with a UV detection technique (Kouvarakis et al., 2002; Salisbury et al. 2003). Meteorological data were measured by both DWD and ECPL using standard instruments. The DWD weather station was mounted on a small mast on top of the container. In the present paper we use the DWD data which were in excellent agreement with the ECPL data.

3. Results and discussion

3.1. General overview and data classification

Figure 1a shows the temporal profile of the ambient air OH concentration at Finokalia for the whole measurement period of 6–12 August 2001. The corresponding ozone photolysis frequency $J(O^1D)$ is shown in Fig. 1b. Pronounced diurnal cycles were observed for both parameters with maximum OH levels occurring roughly between 13:30–14:00 h Greek summer time or 10:30–11:00 UTC (lowest local solar zenith angle). Corresponding OH values (5 min averages) typically peaked in the range of $1.5 - 2.0 \times 10^7\,cm^{-3}$, with individual spikes reaching up to $2.4 \times 10^7\,cm^{-3}$. In general, OH levels at night were below the detection limit. The average OH concentration for the whole measurement period was $4.5 \pm 1.1 \times 10^6\,cm^{-3}$. The noon values of both $J(O^1D)$ and $J(NO_2)$ were in the same range as corresponding values measured in May 2000 at the northwestern coast of Crete (Balis et al., 2002). The latter study was part of the Photochemical Activity and Ultraviolet Radiation (PAUR) campaign and included the only previously reported $J(O^1D)$ and $J(NO_2)$ values measured in the Eastern Mediterranean region.

The results shown in Fig. 1a suggest that the OH data can be classified into different periods. Therefore, we examined individual parameters relevant for the OH balance

ACPD
3, 1183–1212, 2003

such as corresponding CO, O_3, and meteorological data shown in Figs. 2a and 2b. The CO data measured by J. Sciare have been discussed in detail in the companion paper by Salisbury et al. (2003). To provide a clear context for the following discussion we have reproduced them here in Fig. 2b. Based on the above data analysis we divided the OH data set into three major time periods: I: 6–8 August, II: 9–11 August, and III: 13–18 August (Table 1). These overlap with the corresponding periods 2, 3, and 4, respectively, defined by Salisbury et al. (2003). Period III can easily be distinguished from I and II due to relatively enhanced OH values following 12 August. Furthermore, local meteorological conditions significantly changed on 12–13 August showing a transition from southwesterly to northwesterly wind directions and a concurrent drop in wind speed (Fig. 2a). In addition, a significant increase in both absolute humidity (H_2O concentration, Table 1) and relative humidity (Fig. 2b) was observed starting on 12 August, the latter increasing roughly from 30–50% to 60–80%. Also, O_3 mixing ratios dropped from 60–70 to 50–60 ppbv (Fig. 2b). Since 12 August was characterized by significant changes in air mass composition and corresponding OH data are missing for the noontime hours this day has been excluded from the present classification. Also, the end of the campaign (past 18 August) has been excluded due to missing CO data and continuously changing meteorological and atmospheric chemical conditions. Between 9 and 11 August both CO mixing ratios and relative humidity (and also [H_2O]) showed transient maximum values in correlation with the advection of air masses impacted by biomass burning (Salisbury et al., 2003). Therefore, we distinguished this episode as period II. The average OH concentrations corresponding to the three periods defined above were $3.7 \pm 0.7 \times 10^6$ cm^{-3} (I), $4.1 \pm 0.7 \times 10^6$ cm^{-3} (II), and $4.9 \pm 1.0 \times 10^6$ cm^{-3} (III), respectively. In Table 1 statistical results for several parameters with importance for the OH balance are summarized for each of the three periods.

On average, most of the atmospheric chemical observations at Finokalia were consistent with large scale changes in the composition and origin of air masses over the Mediterranean Sea advected to the measurement site. This can be concluded from

ACPD
3, 1183–1212, 2003

a comparison with flight measurements (Traub et al., 2003; de Reus et al., 2003) and from trajectory analyses used to categorize the different air masses by composition and origin (Salisbury et al., 2003). The trajectory analyses showed that the streamlines of air masses approaching the coast of Crete from northerly directions were deflected to a more westerly direction in the vicinity of the coast. In addition, a regular day-night pattern in both wind direction and wind speed was observed at Finokalia corresponding to a land-sea breeze circulation, particularly during the periods I and II and the last days of the campaign (20–22 August). It cannot entirely be excluded that local and regional contributions from Crete may have contributed to the air mass composition measured at Finokalia. However, both NO and CO measurements at the station indicated no major impact from anthropogenic sources on the island, e.g. from Heraklion. Also, this contribution should have been less significant during daytime than at night since the wind was blowing from the sea during daytime. To check for local impacts due to biogenic emissions from the plants, local herb samples were plucked and held into the air sample flow close to the CIMS inlet. Corresponding effects on the measured OH signals were found to be negligible.

Having classified the OH data set into three different periods we now examine for each of these periods the relationship between [OH] and $J(O^1D)$, the latter parameter exhibiting by far the strongest variability in primary OH production (Eq. 1 and Fig. 1b).

3.2. Box model calculations and comparison with empirical approach

The in situ OH concentrations measured at Finokalia (Fig. 1a) represent a quasi-steady state balance between different OH sources and sinks. In the lower troposphere the OH lifetime is typically less than 1 s and photostationary state equilibrium within the HO_x system (= OH + HO_2) is typically achieved within a few minutes (Poppe et al., 1994). Thus, for a typical wind speed of 8 m s^{-1} we may assume that the local OH concentration was determined by the meteorological and atmospheric chemical conditions prevailing within a distance of at most a few km around the station. Complementary to the detailed model study by Baboukas et al. (2003) we focus in this section more explic-

ACPD
3, 1183–1212, 2003

itly on an analysis of the relationship between [OH] and $J(O^1D)$ by means of a simple box model. Using this alternative approach we attempt to identify the photochemical information contained in the variability of the OH data.

First, a visual comparison between Figs. 1a and 1b suggests a high degree of correlation between the OH and $J(O^1D)$ data. Figure 3a shows the corresponding linear regression analysis. However, it is also obvious that the relationship between both data sets is non-linear. As described by Ehhalt and Rohrer (2000), a more realistic fit which also yields a much better correlation is obtained using an exponential relationship:

$$[OH] = a\,J(O^1D)^b. \quad (3)$$

A log-log regression of [OH] vs. $J(O^1D)$ yields a value of $b = 0.68 \pm 0.01$ for the exponent. The same value for the exponent was also found for the data subsets corresponding to each of the three periods defined above. Using this value in combination with Eq. (3), a plot of [OH] vs. $J(O^1D)^{0.68}$ becomes linear with R = 0.953 (Fig. 3b). In the following analysis we want to answer two questions: 1. Can the empirical functional expression (3) and the exponent $b = 0.68$ be explained by our present knowledge of atmospheric photochemistry? 2. How much of the residual variability shown in Fig. 3b can be attributed to the precision of the CIMS instrument, how much to atmospheric variability?

The photochemical balance of OH includes as major sources: the reaction of $O(^1D)$ atoms with H_2O (R3) and the recycling of OH by reaction of HO_2 with NO and ozone (reactions R4 and R5; see also Baboukas et al., 2003). The production of OH through reaction (R3) depends linearly on $J(O^1D)$ because of the strong coupling between reactions (R1), (R2), and (R3). With respect to the HO_2 balance one can distinguish between two extreme conditions: 1. At low NO mixing ratios the loss of HO_2 proceeds mainly via the self-reaction (R8) resulting in a square root dependence of $[HO_2]$ on its production rate, $P(HO_2)$. HO_2 in turn is weakly coupled to the OH concentration through the slow reaction with O_3 (reaction R5). 2. At high NO levels, reaction (R4) is very fast; therefore the coupling between HO_2 and OH is strong resulting in a quasi-

linear relation between [HO_2] and P(HO_2).

Based on these considerations we define three "regimes" determining the dependence of [OH] on J(O^1D) provided that secondary HOx-sources (e.g. the photolysis of aldehydes) can be neglected:

1. Very low NO_x(<10 pptv): The major source of OH is reaction (R3) in which P(OH) depends linearly on J(O^1D). A small amount of OH is produced via the reaction of HO_2 with ozone, which has a square root dependence on the production of HO_2. Overall, we expect a slightly less than linear dependence of [OH] on J(O^1D).

2. Very high NO_x (>10 ppbv): In this case, HO_2 levels should be very low. Again, the major source of OH is reaction (R3) with P(OH) depending linearly on J(O^1D). Overall, we expect a quasi-linear relationship between [OH] and J(O^1D).

3. Moderate NO_x: Here the situation is more complex. The loss of HO_2 is controlled by both reactions (R8) and (R4). The recycling via reaction (R4) is the dominant source of OH. Therefore, J(NO_2) becomes an important parameter because it controls the NO mixing ratio and introduces an additional dependence on solar irradiance. The [OH] vs. J(O^1D) relationship can be less than, equal to, or stronger than linear, i.e. the value of the exponent b in Eq. (3) can range between 0.5 and 1.2 depending on the boundary conditions. For example using an exponent of 1 between J(NO_2) and J(O^1D) in Eq. (4) we calculate a value of b = 1.1.

During MINOS the photochemical conditions corresponded to regime 3) since the mean NO_2 mixing ratio was about 0.5 ppbv (Lange et al., 2003). For a more detailed analysis we applied a simple box model including CO-CH_4-chemistry and followed the analytical procedure described by Ehhalt and Rohrer (2000) with updated kinetic parameters from Sander et al. (2000). The key for understanding the conditions prevailing during MINOS is the relation between the photolysis frequencies J(O^1D) and J(NO_2) which must be explicitly determined. Figure 4 shows a well-defined relationship between J(O^1D) and J(NO_2) which can be explained by the fact that during the whole

MINOS campaign Finokalia station experienced almost always clear sky conditions. The relation between $J(O^1D)$ and $J(NO_2)$ can be approximated by an exponential fit:

$$J(NO_2) \sim J(O^1D)^c. \quad (4)$$

Here the exponent c represents the magnitude of the sensitivity ratio $d\{\ln(J(NO_2))\}/d\{\ln(J(O^1D))\}$. A value of $c = 0.30$ was found for $J(O^1D)$ values larger than $1 \times 10^{-5}\,s^{-1}$ (Fig. 4). This means that if $J(O^1D)$ increases by 1%, $J(NO_2)$ increases by 0.3%. To analyze the functional relationship between measured [OH] and measured $J(O^1D)$ we calculated and added the partial dependences (derivatives) of [OH] on $J(O^1D)$ and of [OH] on $J(NO_2)$, with the latter being weighted by the functional relationship between $J(O^1D)$ and $J(NO_2)$ by the sensitivity of 0.30 (Fig. 4). For average daytime conditions during the MINOS campaign the partial derivatives of [OH] on $J(O^1D)$ and on $J(NO_2)$ were calculated to be 0.5 and 0.6, respectively. Thus, the total sensitivity of measured [OH] vs. measured $J(O^1D)$ during the MINOS campaign was found to be approximately 0.68 (= 0.5 + 0.6 × 0.30). Following Ehhalt and Rohrer (2000), we extended this sensitivity analysis to all relevant photolysis frequencies as defined by the general expression $\partial\{\ln([OH])\}/\partial\{\ln(J)\} \times d\{\ln(J)\}/d\{\ln(J(O^1D))\}$, with $J = J(O^1D)$, $J(NO_2)$, $J(HCHO)$, $J(H_2O_2)$, $J(HONO)$. The individual results were calculated for the average daytime photolysis frequency of $J(O^1D) = 1.3 \times 10^{-5}\,s^{-1}$ and are shown in Fig. 5. Because photolysis frequencies other than $J(O^1D)$ and $J(NO_2)$ were not measured at Finokalia we used their correlation to $J(O^1D)$ as published by Kraus and Hofzumahaus (1998) to estimate $J(HCHO)$, $J(H_2O_2)$, and $J(HONO)$. Mixing ratios of HCHO, H_2O_2, and HONO were not measured at Finokalia. However, we assumed a HCHO value of 1 ppbv corresponding approximately to the mean HCHO mixing ratio obtained from airborne measurements near the station in the lower marine boundary layer (Kormann et al., 2003; Lelieveld et al, 2002a). For H_2O_2 and HONO we calculated steady-state mixing ratios using our model. Based on these approximations we calculated the total dependence of [OH] on $J(O^1D)$, i.e. $d[OH]/d\{J(O^1D)\}$ to be 0.70, which is in quite good agreement to the value of 0.68 derived from the

ACPD
3, 1183–1212, 2003

corresponding measurements.

These values are significantly smaller than the corresponding values determined from the results of the POPCORN campaign (0.92 from measurements and 0.85 from model calculations, respectively; Ehhalt and Rohrer, 2000). This can be largely explained by significantly different radiation conditions during both campaigns yielding very different overall relationships between $J(O^1D)$ and $J(NO_2)$. In contrast to MINOS, overcast conditions dominated most of the measurement period during POPCORN. In general, for the relatively few days with clear sky conditions an exponent of 0.3 was obtained from Eq. (4) which changed to 1 for days with total cloud coverage. During MINOS, short-term transient cloud passages over the measurement site occurred on a few days. As shown in Fig. 4, the corresponding relatively small subset of data clearly deviates from the regression curve and, similar to POPCORN, suggests a near-unity exponent (quasi-linear relation) between $J(O^1D)$ and $J(NO_2)$ for these conditions. The average value for the corresponding exponent c determined from the total POPCORN results using Eq. (4) was 0.50 (Ehhalt and Rohrer, 2000) in contrast to the value of 0.30 resulting from the MINOS campaign which was dominated by clear sky conditions. Based on these results, for the relation between [OH] and $J(O^1D)$ a slightly higher value of b was modelled for the POPCORN data (b = 0.85) compared to the MINOS data (b = 0.70).

The total [OH] and $J(O^1D)^{0.68}$ data from MINOS were strongly correlated (R = 0.953). Based on our estimated precision of the CIMS instrument (Sect. 2.1) one could expect a maximum correlation with R_{max} = 0.986. The difference between the two R-values can be explained by the variability of components in the data record other than the relation between [OH] and $J(O^1D)$. This can be estimated to contribute 6% ($= 0.986^2 - 0.953^2$) to the total variance of [OH]. To identify the cause of this difference we divided the OH dataset into three periods as shown in Table 1. We calculated three individual correlation coefficients between OH and $J(O^1D)^{0.68}$ and found corresponding correlation coefficients of R_I = 0.982, R_{II} = 0.988, and R_{III} = 0.980, each of which are very close to R_{max} = 0.986. This means that for each of the three time pe-

ACPD
3, 1183–1212, 2003

riods the variability of the measured [OH] data is almost completely explained by the variance of $J(O^1D)$ and the precision of the CIMS instrument. Only 1% of the total variance in [OH] remains unexplained. Most of this remainder can be attributed to 8 obvious outliers out of the 2500 OH data points (Fig. 1a). These 8 data points show the highest OH concentrations above 2×10^7 cm^{-3}. At least in some cases these may have been caused by local emissions of NO from cars occasionally passing the site (see also Salisbury et al., 2003). However, the number of these outliers is small enough to fall just into the allowed limits of a normal distribution.

In summary, from the above analysis we could derive and quantify four principal parameters characterizing the relationship observed between [OH] and $J(O^1D)$, namely the exponent b and three different scaling factors a_{I}, a_{II}, and a_{III} for the corresponding time periods to be used in conjunction with Eq. (3). We now apply these quantitative results to normalize the data set. For this, we divide each [OH] value by the appropriate a_j and scale so that the average of $[OH]_{CIMS}$ is maintained: $[OH]_{norm} = ([OH]_{CIMS,i}/a_j)/\sum([OH]_{CIMS,i}/a_j) \times \sum([OH]_{CIMS,i})$. Here $[OH]_{CIMS,i}$ denotes the individual [OH] data points, a_j the corresponding experimental scaling factor taken from Table 2. The result of this normalizing procedure for the time period 6–18 August 2001 is shown in Fig. 6. The correlation coefficient between $[OH]_{norm}$ and $J(O^1D)^{0.68}$ is $R_{norm} = 0.983$ which is very close to the maximum possible value $R_{max} = 0.986$ (see above). The comparison between Fig. 6 and Fig. 3b clearly demonstrates the extent at which this normalization using b and the three parameters a_{I}, a_{II}, and a_{III} has reduced the variance in the [OH] data set.

A comparison of this result with model calculations of [OH] using measured photolysis frequencies and boundary conditions, is essentially a comparison pertaining to these four quantities a_{I}, a_{II}, a_{III} and b. As explained above, the exponent b gives information about the different production terms of OH. The pre-exponential factor a represents the combination of boundary conditions like mixing ratios of ozone, CO, NMHC, HCHO etc. and kinetic parameters. Using the present approach one can check the combination of these quantities within the limit given by the accuracy of the

ACPD
3, 1183–1212, 2003

CIMS instrument. However, even with the very good precision of the CIMS instrument this does not permit an evaluation of the contributions from individual photochemical processes determining the concentration of OH during the MINOS campaign. Therefore, we also performed box model calculations using the CO/CH_4-model described in Ehhalt and Rohrer (2000). We calculated three different diurnal cycles with average boundary conditions given in Table 1, diurnal cycles of measured $J(O^1D)$ and $J(NO_2)$ taken from the very first day of each of the three time periods, and estimated CH_4, H_2, and HCHO mixing ratios of 1900 ppbv, 550 ppbv, and 1 ppbv, respectively.

The experimental and model calculated pre-exponential factors a_{I}, a_{II}, and a_{III} are given in Table 2. The individual values are in agreement with each other within the accuracy of the CIMS instrument of 20%. On average, the difference between the results obtained from the measurements and the model calculations is 7%. The major experimental uncertainty seems to be the mixing ratio of NO_2. Changing NO_2 in the model calculations within the 18- and 82-percentile values given in Table 1 changes [OH] by about a factor of 1.5 higher or lower. On the other hand, the correlation analysis discussed above showed that no major processes have been missed to explain the variability of the measured OH concentration. Therefore, the NO_2 mixing ratio should have been relatively constant within each of the three time periods. As a consequence, the 18- and 82-percentile values of NO_2 shown in Table 1 seem to reflect mainly the experimental precision of the NO_2 measurements (Lange et al., 2003) than the variability of atmospheric NO_2 levels.

Equation (3) can be used to empirically interpolate the OH data based on the corresponding exponential and pre-exponential values. Taking the experimental a-values given in Table 2 and an exponent of 0.68 we calculated a continuous time series of [OH] for the period of 6–18 August (Fig. 7). On 12 August a gap in the OH data occurred due to technical problems. Since the air mass characteristics changed on that day we calculated two corresponding OH profiles using a_{II} and a_{III}, respectively. The two profiles included in Fig. 7 demonstrate the resulting difference from using either value. Overall, the agreement between the empirical calculation and the measured OH

ACPD
3, 1183–1212, 2003

data is very good. The discussion above has shown that the difference between both the measured and calculated OH data is in the range of the estimated accuracy of the CIMS instrument.

4. Conclusions

As part of the MINOS campaign we have conducted highly time-resolved measurements of atmospheric OH, H_2SO_4, and methanesulfonic acid (MSA) concentrations at Finokalia Station on the northeastern coast of Crete. The sulfur gas measurements are reported in the companion paper by Bardouki et al. (2003). In the present study we have evaluated the results of the OH measurements in conjunction with $J(O^1D)$ and $J(NO_2)$ photolysis frequencies, mixing ratios of O_3, NO_x, and CO, and meteorological data measured at the site. Similar to $J(O^1D)$, the OH levels showed a strong diel variation with peak values of approximately 2×10^7 molecules cm^{-3}. The mean OH concentration for the total measurement period (6–21 August 2001; 0–24 h data) was $4.5 \pm 1.1 \times 10^6$ molecules cm^{-3} which is significantly higher than the zonal (36° N) and monthly (July) averaged value of 1.5×10^6 cm^{-3} (at 1000 hPa) calculated by Spivakovsky et al. (2000) using a global 3D-model.

However, our measured OH data are in close agreement with the MINOS model studies by Baboukas et al. (2003) and Kanakidou et al. (2003). In the present work we show that they are also consistent with the results from a relatively simple box model including CH_4-CO-photochemistry. We have used a systematic approach based on the work of Ehhalt and Rohrer (2000) to analyze the [OH] vs. $J(O^1D)$ relationship. Three time periods during the campaign could be distinguished. For each of these periods we inferred the relationship between [OH] and $J(O^1D)$ using the empirical function $[OH] = a\ J(O^1D)^b$ and explicitly determined the effect of $J(NO_2)$ on this relationship. The corresponding pre-exponential factors a_{I}, a_{II} a_{III} and the exponent b (whose value turned out to be the same for all three periods) were used in a normalization procedure to describe a fit to the total [OH] data series (except for transition periods). A very good

ACPD
3, 1183–1212, 2003

fit to the measured data was obtained. The major surprising result of this analysis was that the variance in the normalized [OH] data could nearly be fully explained (99%) by the variability of $J(O^1D)$ (inherently including a small but significant contribution by $J(NO_2)$) and the precision of the CIMS measurements.

Based on the value of 0.68 obtained for the exponent b the major sources of OH were found to be ozone photolysis and recycling of OH via the HO_2+NO reaction. This means that other processes influencing the local OH production were unimportant which is in agreement with the model results by Baboukas et al. (2003). Differences in boundary conditions, e.g. mean mixing ratios of NO, O_3, water vapor, and CO during the three time periods are represented here by the three pre-exponential factors a_{I}, a_{II}, and a_{III}, respectively.

In conclusion, we recommend that future studies of this kind should include measurements of all parameters expected to be of potential importance for the local OH balance at a particular field site, especially photolysis frequencies and NO and NO_2 mixing ratios. Furthermore, to detect and quantify different contributions to the OH balance all corresponding measurements including those of OH need to be made with a sufficiently high degree of precision and accuracy. It will be interesting to test the present empirical approach in further field studies and to determine the degree of complexity of both measurements and model calculations required for reproducing locally measured OH concentrations.

Acknowledgement. We thank J. Lelieveld for the opportunity to participate in MINOS, and M. de Reus and P. Petsalakis for their organizational and logistical help. We are also indebted to the MPI and ECPL teams for their help at Finokalia and collection of data contributing to this work, and especially to G. Stange for his valuable assistance in carrying out the DWD's measurements. Furthermore, we thank J. Sciare for communicating his CO data, B. Bohn for his excellent job in calibrating the $J(O^1D)$ instrument, and E. Baboukas, M. Lawrence, and D. Poppe for helpful discussions. This work was financially supported by the Max-Planck Society (MPG) and the German Weather Service (DWD/BMVBW).

References

Baboukas, E., Berresheim, H., Kanakidou, M., Lawrence, M., and Lelieveld, J.: Modeling of OH levels during the MINOS campaign and comparison with measurements, Atmos. Chem. Phys., submitted, 2003.

Balis, D. S., Zerefos, C. S., Kourtidis, K., Bais, A. F., Hofzumahaus, A., Kraus, A., Schmitt, R., Blumthaler, M. and Gobbi, G. P.: Measurements and modeling of photolysis rates during the Photochemical Activity and Ultraviolet Radiation (PAUR) II campaign, J. Geophys. Res., 107, 8138, 10.1029/2000JD000136, 2002.

Bardouki, H., Berresheim, H., Sciare, J., Kouvarakis, G., Vrekoussis, M., Economou, C., and Mihalopoulos, N.: Gaseous (DMS, MSA, SO_2, H_2SO_4 and DMSO) and particulate (sulfate and methanesulfonate) sulfur species during the MINOS campaign: 1. Experimental data, Atmos. Chem. Phys., submitted, 2003.

Berresheim, H., Elste, T., Plass-Dülmer, C., Eisele, F. L., and Tanner, D. J.: Chemical ionization mass spectrometer for long-term measurements of atmospheric OH and H_2SO_4, Int. J. Mass Spectrom., 202, 91–109, 2000.

Cantrell, C. A., Zimmer, A., and Tyndall, G. S.: Absorption cross sections for water vapor from 183 to 193 nm, Geophys. Res. Lett., 24, 2195–2198, 1997.

Ehhalt, D. H. and Rohrer, F.: Dependence of the OH concentration on solar UV, J. Geophys. Res., 105, 3565–3571, 2000.

Eisele, F. L. and Tanner, D. J.: Ion-assisted tropospheric OH measurements, J. Geophys. Res., 96, 9295–9308, 1991.

Kanakidou, M., Vrekoussis, M., Berresheim, H., Bardouki, H., Sciare, J., Kouvarakis, G., Economou, C., Schneider, J., Borrmann, S., and Mihalopoulos, N.: Gaseous (DMS, MSA, SO2, H2SO4, and DMSO) and particulate (sulfate and methanesulfonate) sulfur species during the MINOS campaign: 2. A modelling approach, Atmos. Chem. Phys., submitted, 2003.

Kormann, R., Fischer, H., de Reus, M., Lawrence, M., Brühl, C., von Kuhlmann, R., Warneke, C., de Gouw, J., Schlager, H., Ziereis, H., Heland, J., Holzinger, R., Williams, J., and Lelieveld, J.: Formaldehyde over the Eastern Mediterranean during MINOS: Comparison of airborne in- situ measurements with 3D-model results, Atmos. Chem. Phys., submitted , 2003.

Kouvarakis, G., Vrekoussis, M., Mihalopoulos, N., Kourtidis, K., Rappenglück, B., Gerasopou-

los, E., and Zerefos, C.: Spatial and temporal variability of tropospheric ozone (O_3) in the boundary layer above the Aegean Sea (Eastern Mediterranean), J. Geophys. Res., 107, D18, 10.1029/2000JD000081, 2002.

Kraus, A. and Hofzumahaus, A., Field measurements of atmospheric photolysis frequencies for O_3, NO_2, HCHO, CH_3CHO, H_2O_2, and HONO by UV spectroradiometry, J. Atmos. Chem., 31, 161–180, 1998.

Lange, L., Williams, J., Lawrence, M., von Kuhlmann, R V., Vrekoussis, M., Economou, C., Mihalopoulos, N., and Lelieveld, J.: The budget of reactive nitrogen species at a ground based station on Crete during the MINOS 2001 campaign, Atmos. Chem. Phys., submitted, 2003.

Lelieveld, J., Berresheim, H., Borrmann, S., Crutzen, P. J., Dentener, F. J., Fischer, H., de Gouw, J., Feichter, J., Flatau, P., Heland, J., Holzinger, R., Korrmann, R., Lawrence, M., Levin, Z., Markowicz, K., Mihalopoulos, N., Minikin, A., Ramanathan, V., de Reus, M., Roelofs, G. J., Scheeren, H. A., Sciare, J., Schlager, H., Schultz, M., Siegmund, P., Steil, B., Stephanou, E., Stier, P., Traub, M., Williams, J. and Ziereis, H.: Global air pollution crossroads over the Mediterranean, Science, 298, 794–799, 2002a.

Lelieveld, J., Peters, W., Dentener, F. J., and Krol, M. C.: Stability of tropospheric hydroxyl chemistry, J. Geophys. Res., 107, 10.1029/2002JD002272, 2002b.

Matsumi, Y., Comes, F. J., Hancock, G., Hofzumahaus, A., Hynes, A. J., Kawasaki, M., and Ravishankara, A. R.: Quantum yields for production of O(1D) in the ultraviolet photolysis of ozone: Recommendation based on evaluation of laboratory data, J. Geophys. Res., 107, D3, 10.1029/2001JD000510, 2002.

Platt, U., Alicke, B., Dubois, R., Geyer, A., Hofzumahaus, A., Holland, F., Martinez, M., Mihelcic, D., Klüpfel, T., Lohrmann, B., Pätz, W., Perner, D., Rohrer, F., Schäfer, J., and Stutz, J.: Free radicals and fast photochemistry during BERLIOZ, J. Atmos. Chem., 42, 359–394, 2002.

Poppe, D., Zimmermann, J., Bauer, R., Brauers, T., Brüning, D., Callies, J., Dorn, H.-P., Hofzumahaus, A., Johnen, F.-J., Khedim, A., Koch, H., Koppmann, R., London, H., Müller, K.- P., Neuroth, R., Plass-Dülmer, C., Platt, U., Rohrer, F., Röth, E.-P., Rudolph, J., Schmidt, U., Wallasch, M. and Ehhalt, D. H.: Comparison of measured OH concentrations with model calculations, J. Geophys. Res., 99, 16633–16642, 1994.

de Reus, M., Fischer, H., Arnold, F., de Gouw, J., Warneke, C., and Williams, J.: On the relationship between acetone and carbon monoxide in different air masses, Atmos. Chem. Phys. Discuss., 3, 1017–1049, 2003.

Salisbury, G., Williams, J., Holzinger, R., Gros, V., Mihalopoulos, N., Vrekoussis, M., Sarda-Esteve, R., Berresheim, H., von Kuhlmann, R., Lawrence, M., and Lelieveld, J.: Ground-based PTR-MS measurements of reactive organic compounds during the MINOS campaign in Crete, July–August 2001, Atmos. Chem. Phys. Discuss., 3, 911–948, 2003.

Sander, S. P., Friedl, R. R., DeMore, W. B., Golden, D. M., Kurylo, M. J., Hampson, R. F., Huie, R. E., Moortgat, G. K., Ravishankara, A. R., Kolb, C. E., and Molina, M. J.,: Chemical kinetics and photochemical data for use in stratospheric modeling, JPL Publ. 00-3, 13, 2000.

Spivakovsky, C. M., Logan, J. A., Montzka, S. A., Balkanski, Y. J., Foreman-Fowler, M., Jones, D. B. A., Horowitz, L. W., Fusco, A. C., Brenninkmeijer, C. A. M., Prather, M. J., Wofsy, S. C. and McElroy, M. B.: Three-dimensional climatological distribution of tropospheric OH: Update and evaluation, J. Geophys. Res., 105, 8931–8980, 2000.

Tanner, D. J., Jefferson, A., and Eisele, F. L.: Selected ion chemical ionization mass spectrometric measurement of OH, J. Geophys. Res., 102, 6415–6425, 1997.

Traub, M., Fischer, H., de Reus, M., Kormann, R., Heland, J., Ziereis, H., Schlager, H., Holzinger, R., Williams, J., Warneke, C., de Gouw, J., and Lelieveld, J.: Chemical characteristics assigned to trajectory clusters during the MINOS campaign, Atmos. Chem. Phys. Discuss., 3, 107-134, 2003.

Table 1. Median daytime (03:50–16:50 UTC) levels of atmospheric trace gases and meteorological parameters measured during MINOS. The data are classified into three periods as defined in the text. Numbers in parentheses show corresponding 18- and 82-percentile values

Parameter	Period I 6–8 August	Period II 9–11 August	Period III 13–18 August
CO, ppbv	130 (115, 146)	228 (189, 246)	161 (145, 174)
O_3, ppbv	61 (54, 65)	67 (64, 70)	56 (52, 58)
NO_2, ppbv	0.34 (0.06, 0.47)	0.36 (0.15, 0.53)	0.66 (0.41, 1.04)
Temperature, $^\circ$C	27.8 (26.2, 29.3)	28.1 (27.3, 29.4)	24.9 (24.2, 25.4)
H_2O, 10^{17} cm^{-3}	3.5 (3.2, 4.0)	4.8 (3.9, 5.3)	5.5 (5.2, 5.8)
$J(O^1D)$, 10^{-5} sec^{-1}	1.2 (0.16, 2.4)	1.1 (0.13, 2.1)	0.83 (0.10, 2.0)
$J(NO_2)$, 10^{-3} sec^{-1}	7.9 (3.7, 9.5)	7.3 (3.0, 9.0)	7.4 (2.4, 9.3)

Table 2. Experimental and model calculated slope of the function [OH] = a $J(O^1D)^{0.68}$ for the three time periods of the MINOS campaign as defined in Table 1. Also given are the correlation coefficients between $[OH]_{CIMS}$ and $J(O^1D)^{0.68}$ and the result of additional model calculations using the lower and the upper bound of NO_2 concentrations given in Table 1

Parameter	Period I 6–8 August	Period II 9–11 August	Period III 13–18 August
$R([OH]_{CIMS}, J(O^1D)^{0.68})$	0.982	0.988	0.980
a(experiment)/$\times 10^{10}$ s cm^{-3}	1.39	1.71	2.20
a(model)/$\times 10^{10}$ s cm^{-3}	1.65	1.49	2.44
a(model)/a(experiment)	1.19	0.87	1.11
a(model) NO_2 lower bound	0.92	1.08	1.95
a(model) NO_2 upper bound	1.91	1.78	2.78

ACPD
3, 1183–1212, 2003

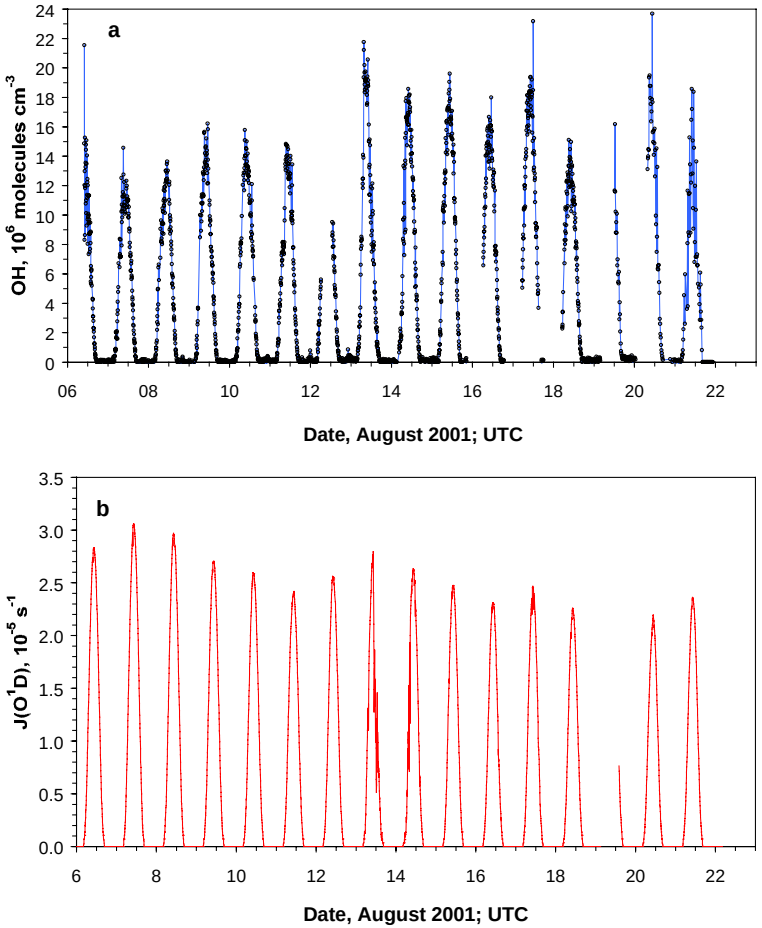

Fig. 1. (a) OH concentration and **(b)** ozone photolysis frequency (upper 2π sr +10% from lower 2π sr; see text) measured concurrently at Finokalia Station during the MINOS campaign. Dots indicate individual 5 min averaged data.

ACPD
3, 1183–1212, 2003

OH in the coastal boundary layer of Crete during MINOS

H. Berresheim et al.

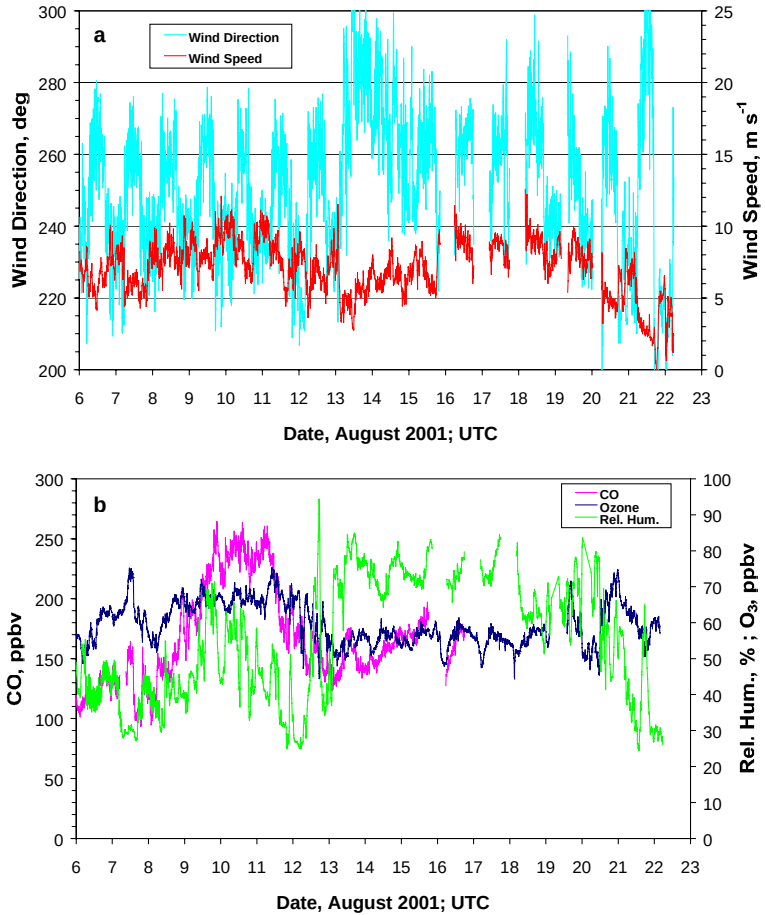

Fig. 2. (a) Local wind direction and wind speed, **(b)** relative humidity and ozone and CO mixing ratios at Finokalia during the MINOS campaign. The CO data were measured by J. Sciare and are reproduced here from the companion paper by Salisbury et al. (2003).

ACPD
3, 1183–1212, 2003

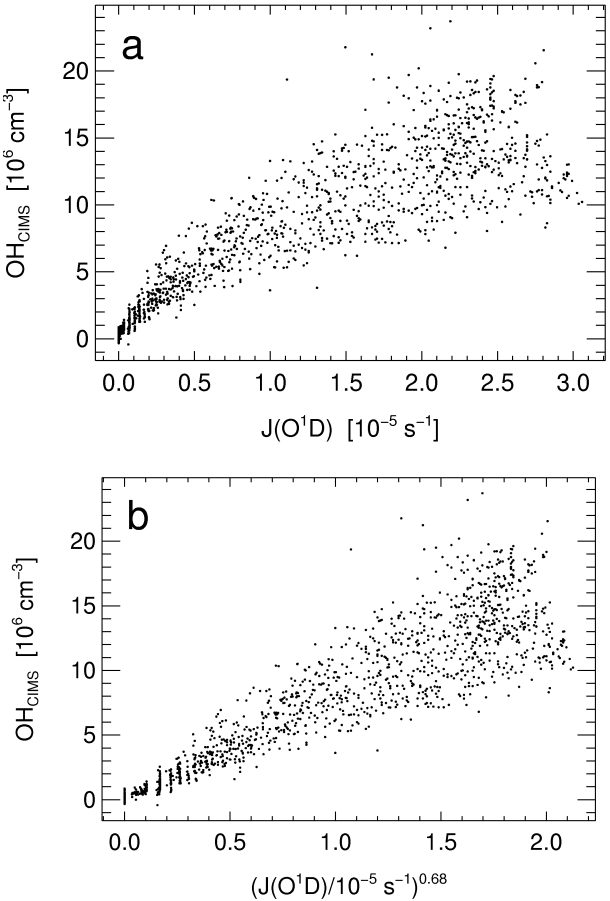

Fig. 3. (a) OH concentrations plotted as a function of $J(O^1D)$ for the whole measurement period (6–22 August 2001). **(b)** Plot of [OH] vs. $J(O^1D)^{0.68}$ yielding a correlation coefficient of 0.953.

ACPD
3, 1183–1212, 2003

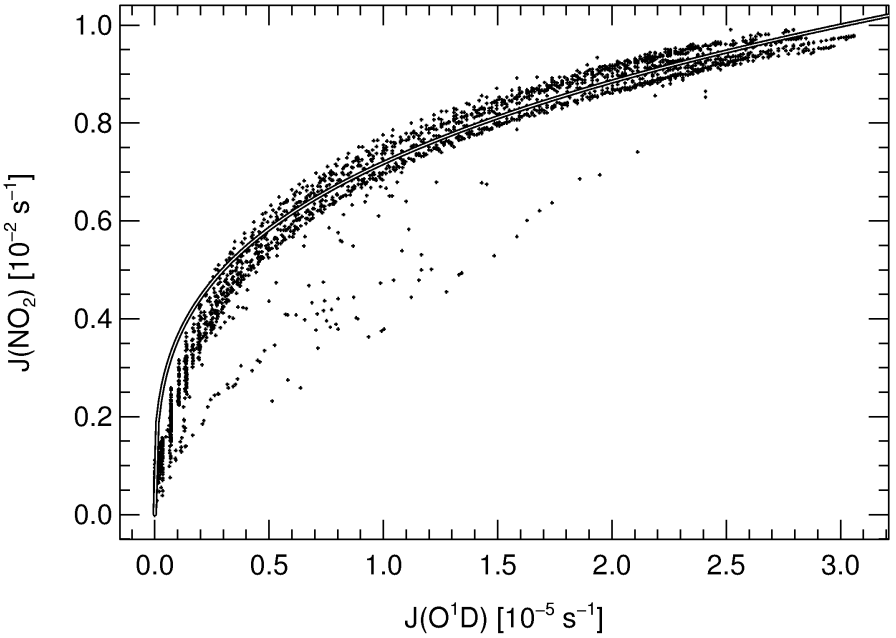

Fig. 4. Scatter plot of measured $J(O^1D)$ vs. $J(NO_2)$ for the MINOS-campaign. The line represents the function $J(NO_2) \sim J(O^1D)^{0.30}$.

ACPD
3, 1183–1212, 2003

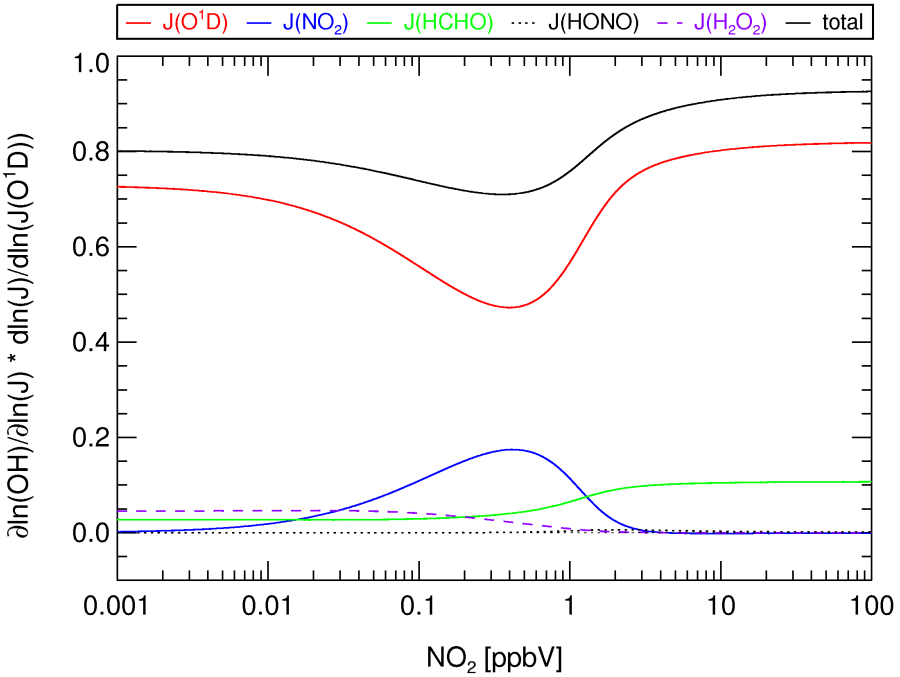

Fig. 5. Sensitivities of [OH] with respect to different photolysis processes vs. NO_2.

ACPD
3, 1183–1212, 2003

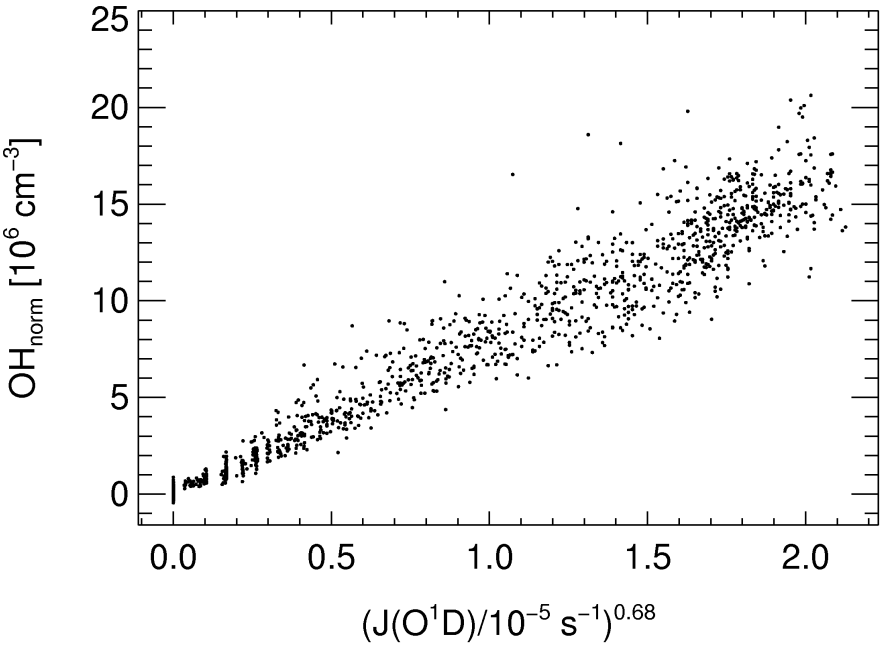

Fig. 6. Normalized [OH] vs. $J(O^1D)^{0.68}$ for the time period 6–18 August 2001. OH_{norm} is calculated using the parameters a_I, a_{II}, a_{III} shown in Table 2 (see text). The corresponding correlation coefficient is 0.983.

ACPD
3, 1183–1212, 2003

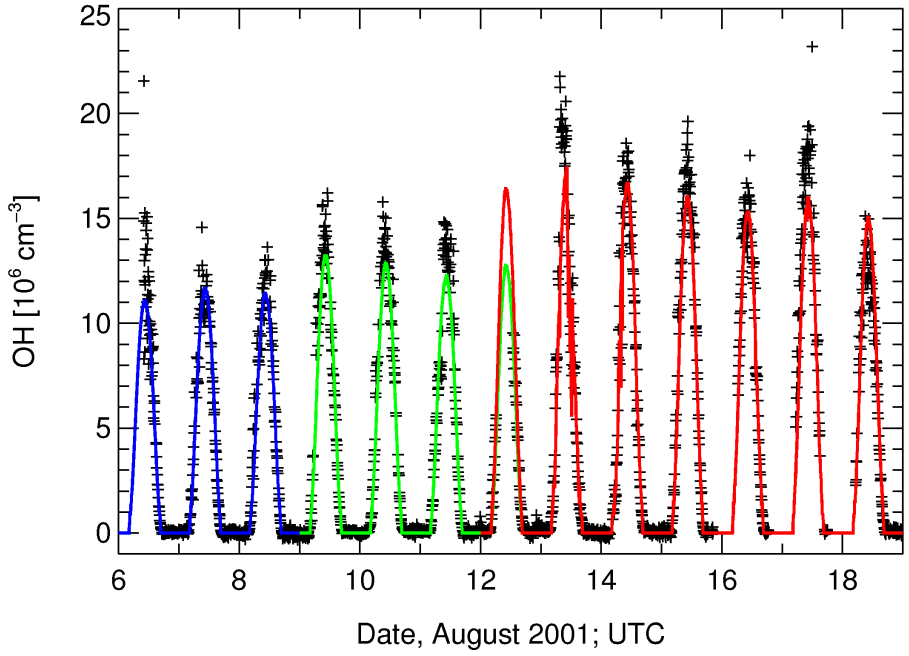

Fig. 7. $[OH]_{CIMS}$ (crosses) and empirical [OH] calculated from Eq. (3) and scaling factors given in Table 2 (blue, green, and red line with a_I, a_{II}, and a_{III}, respectively).

ACPD
3, 1183–1212, 2003